Journal of Materials Chemistry A



PAPER

View Article Online
View Journal | View Issue



Cite this: J. Mater. Chem. A, 2021, 9, 9798

Received 3rd February 2021 Accepted 29th March 2021

DOI: 10.1039/d1ta01007g

rsc li/materials-a

Sunlight-activated phase change materials for controlled heat storage and triggered release†

Yuran Shi, Mihael A. Gerkman, Qianfeng Qiu, Shuren Zhang and Grace G. D. Han 10 *

We report the design of photo-responsive organic phase change materials that can absorb filtered solar radiation to store both latent heat and photon energy *via* simultaneous phase transition and photo-isomerization. The activation of photo-switches by long wavelengths ≥530 nm in the visible light range at a low irradiance is achieved, in the absence of high-intensity light sources, by the *ortho*-substitution of azobenzene units. The facile transition from crystalline to liquid phase is enabled by appending an aliphatic group on the photochromic moiety. The sunlight-activated liquid phase exhibits an exceptionally long heat storage without crystallization for nearly two months, and the release of energy is triggered by a short irradiation at 430 nm. The successful demonstration of photo-controlled latent heat storage accomplished by solar irradiation opens a new horizon on solar energy harvesting by functional organic materials, as a complementary system to photocatalysts and photovoltaic materials.

1. Introduction

Photo-induced molecular transformations, either photochemical reactions¹⁻⁴ or reversible photo-mechanical isomerizations,5-15 have attracted significant attention as a potential chemical method for harnessing solar energy. A particular class of molecules, called molecular solar thermal storage (MOST) systems, 16-18 that respond to light by conformational and energetic changes present an exciting opportunity to store photon energy in constrained chemical bonds and release the energy upon triggering in the form of heat. The absence of byproducts, the capability of isomerizing in condensed phases (i.e. solid and liquid), and recyclability are unique characteristics of the MOST systems, which indicates the potential of applying the molecular systems for a thermal battery. However, the low energy storage density of common MOST compounds, particularly azobenzene derivatives, in the range of \sim 41 kJ mol⁻¹ for pristine,19 remains a challenge for achieving a high-density thermal energy storage for practical applications.

Among various strategies to address this challenge, the promotion of simultaneous isomerization and phase transition between solid and liquid demonstrated to enhance the total energy storage in MOST systems significantly.²⁰ Many material systems including ionic crystals,²¹ self-assembling structures,²² and polymers^{23–25} that incorporate azobenzene switches showed the solid-to-liquid transition while a photo-switch transforms from a planar isomer to a non-planar counterpart.²⁶ More

Department of Chemistry, Brandeis University, 415 South Street, Waltham, MA 02453, USA. E-mail: gracehan@brandeis.edu

 \dagger Electronic Supplementary Information (ESI) available. See DOI: $10.1039/\mathrm{d}1ta01007\mathrm{g}$

recently, azobenzenes or arylazopyrazoles decorated with phase transition-directing alkyl chains manifested both the photon energy storage through E–Z isomerization and the latent heat storage via concomitant melting, followed by the preservation of Z liquid phase in dark.^{27–32}

All of the aforementioned molecular systems, however, share a critical limitation: the E-to-Z switching requires a strong UV irradiation for promoting π - π * transition, which precludes the photo-activation of MOST systems by direct or filtered sunlight. The visible light photons, a major part of solar spectrum, induce Z-to-E reversion of switches, establishing a low % Z in the compounds at the photostationary state. Due to the small fraction (4.5%) of UV photons in the solar spectrum,24 the usage of UV band-pass filters significantly reduces the total irradiance of incident light, resulting in the insufficient *E*-to-*Z* conversion. Fortunately, the ortho-functionalization of azobenzene moiety with fluorine,33 methoxy,34,35 and mixed halogen groups66 have been recently reported to successfully red-shift the $n-\pi^*$ band of E isomers via the intramolecular interaction between the N=N group and the *ortho*-functional groups. The syntheses and solution-state characterizations of such switches have been comprehensively investigated, while the utilization of their remarkable optical properties for the direct harnessing of solar photons has been rarely explored in condensed phases.

A previous work by Wu, *et al.* successfully probed the potential of harnessing solar spectrum by an amorphous polymer functionalized with *o*-methoxy azobenzene side groups, utilizing a Coumarin 314 filter.²⁴ The photo-switching, however, was only demonstrated within extremely thin films (20 nm), and no phase transition was observed, which intrinsically differs from our strategy that takes advantage of latent heat storage in phase change MOST materials at a much larger scale. Various

norbornadiene-based MOST compounds16 have been also investigated for direct sunlight absorption, but no concurrent phase transition has been achieved, as a result of the relatively small geometrical change of such molecules.

Herein, we report the first demonstration of spontaneous solar activation of azobenzene derivatives that undergo the simultaneous phase transition from solid to liquid and the isomerization from E to Z structures. Various ortho-functionalized azobenzene derivatives show the significantly red-shifted $n-\pi^*$ absorption, which allows for the efficient E-to-Z switching under filtered sunlight without the need for any external UV light sources. The appended tridecanoate and ethylhexanoate groups along with the ortho-substituents play an important role in reducing the melting points of the compounds, accomplishing the solid-to-liquid phase transition under the filtered sunlight during the photo-switching process. The liquid phase of Z isomers exhibits an exceptional stability under a wide range of temperatures, -40 °C to 110 °C, successfully storing the latent heat and photon energy for nearly two months, until the specific optical triggering leads to the immediate crystallization and release of heat. This new generation of optically-controlled phase change materials will shed light on the ways in which solar energy is harvested and stored in a large quantity by optically-responsive organic compounds, complementary to organic photovoltaics and photocatalysts.

2. Results and discussion

The photo-controlled phase change materials (PCMs) reported so far have a common molecular structure, i.e. a photo-switch head group linked to an aliphatic tail. This structure creates the balance between the π - π interaction among the head

groups and the London dispersion forces among the tail groups. Such a molecular design allows for the phase transition of molecules, mainly controlled by the conformational change of photo-switches between planar and non-planar geometries and the altered degree of head group interactions. In the recent works that demonstrated the concept of photo-controlled heat storage in organic PCMs, the crystalline PCMs were irradiated with strong UV light using an arc lamp or an LED to undergo photo-switching and simultaneous melting. 27-32,37 Occasionally, the photo-thermal effect of strong UV irradiation promoted the direct photo-melting, while other times external thermal energy input was required to pre-melt the crystalline PCMs to allow for the facile conformational change of the photo-switches. The resulting liquid PCMs have shown a remarkable stability over a large window of temperatures such as −30 °C to 60 °C,²⁸ enabling the long-term storage of latent heat (up to a few weeks) in the photo-activated liquid and the triggered release of the stored heat by optical stimulation within a visible-light range.

In Fig. 1a, a new material system that harnesses solar heat and photon without any external light source or heat source is introduced. The organic PCMs containing planar photoswitches in the ground state (OFF state) initially form crystalline solid that absorbs solar thermal energy and isomerizes by solar photons to result in a liquid phase. The liquid PCMs consisting of non-planar photo-switches in the metastable state (ON state) can be preserved over a substantial range of temperatures, $-40~^{\circ}\text{C}$ to 110 $^{\circ}\text{C}$, until the optical triggering immediately crystallizes the PCMs to release the latent heat. Fig. 1b shows the structural change of a photo-switchable PCM molecule incorporating a novel head group, o-fluoroazobenzene, and a fatty ester tail. The red-shifted $n-\pi^*$

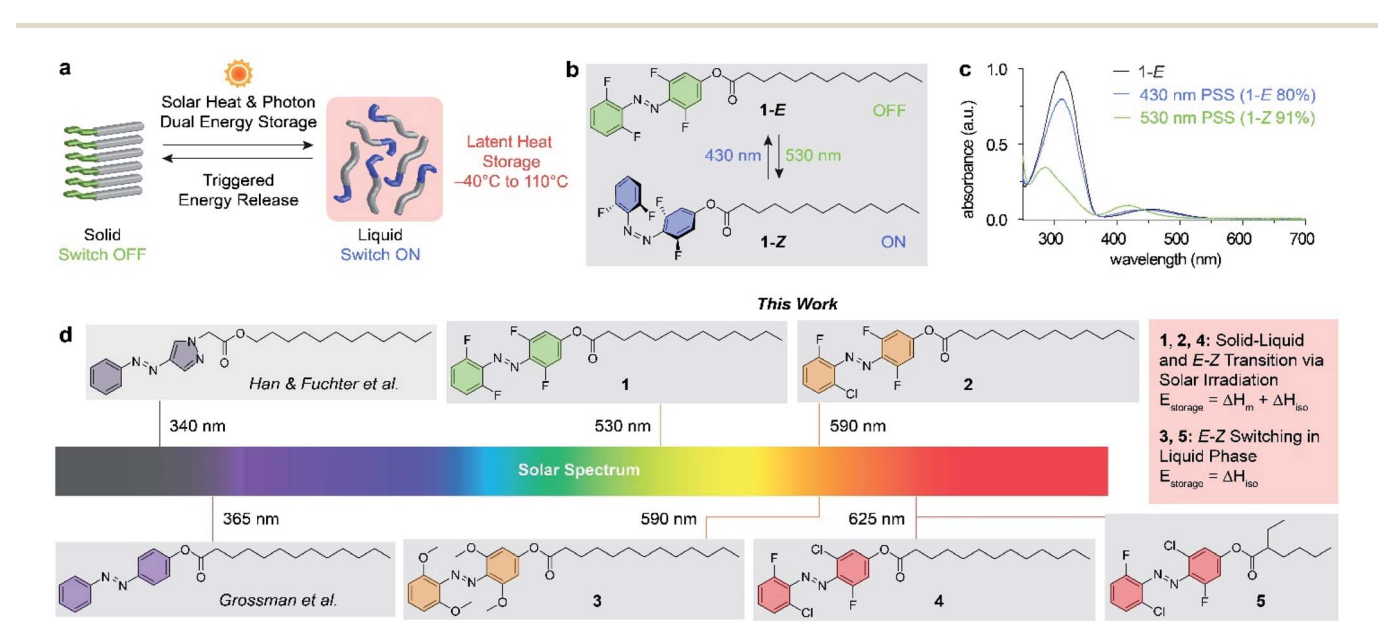


Fig. 1 (a) The operation principle of solar heat and photon energy storage by photo-switchable organic PCMs. (b) Reversible structural isomerization of compound 1 by photo-irradiation. (c) UV-vis absorption spectra of as-synthesized compound 1 (1-E) as well as the compound at the respective photostationary state under 430 nm and 530 nm irradiation. (d) Chemical structures of photo-switchable PCMs either developed in this work (compounds 1–5) or previously reported. The wavelength that maximizes E-to-Z isomerization of each compound is listed. E_{storage}: total energy storage, $\Delta H_{\rm m}$: melting enthalpy, $\Delta H_{\rm iso}$: isomerization enthalpy.

Fig. 1d illustrates the wavelengths of light that induces *E*-to-*Z* isomerization of each azobenzene derivative shown. The pristine azobenzene functionalized with a tridecanoate chain is primarily activated by 365 nm irradiation, as previously reported by Grossman and coworkers in their first demonstration of photo-controlled latent heat storage in organic PCMs.³⁷ In addition, similar structures of pristine azobenzene functionalized with alkyl ether or alkyl ester groups reported by Feng et al. also used 365 nm UV light for E-to-Z isomerization. 30-32 Arylazopyrazole derivatives reported by Han, Fuchter, and coworkers showed the most facile E-to-Z switching by 340 nm activation.²⁸ Another class of arylazopyrazoles functionalized with alkyl ether groups responded to 365 nm as reported by Li, Moth-Poulsen, and the team.27 As all of the reported photo-switchable PCMs require a high-intensity UV light source for initial activation, which is not achieved by solar irradiation, we developed a new series of molecules that undergo E-to-Z isomerization by visible light irradiation.

We designed and synthesized five compounds and demonstrated the viability of sunlight-driven molecular isomerization and concomitant crystal-to-liquid phase transition (compounds 1, 2, and 4), which leads to the storage of both isomerization energy and latent heat. This class of compounds displays a unique phase in each isomeric state (E or Z), exhibiting a phase transition upon photo-induced structural isomerization. We also identified a different class of switches (compounds 3 and 5) that undergo a same-phase photo-switching under sunlight and store the isomerization energy. The respective UV-vis absorption spectra of all compounds in E and Z isomeric forms are shown in Fig. S1.† Compounds 1-5 show excellent reversible isomerization over 30 cycles upon the exposure to alternating irradiation at 530 nm and 430 nm. They

Table 1 Phase change temperatures of compounds $1-5^a$

	E		Z	
	T_{m} (°C)	T_{c} (°C)	T_{m} (°C)	T _c (°C)
1	45	25	$-36 \\ 22'$	$-40 \\ -28^{\rm cc}$
2	56	21	-42	
3	70	16 ^{cc1} 50 ^{cc2} 58 ^{cc3}	106	-47 41 ^{cc}
4	78	37	Liq	Liq
5	9	-1^{cc}	Liq	Liq

 $[^]a$ $T_{\rm m}$: melting point, $T_{\rm c}$: crystallization point, cc: cold-crystallization, ': second melting point.

also exhibit a high photo-stability under the continuous irradiation by 530 nm LED over 15 hours, displaying a minimal photo-degradation in the range of 0.2–3.2% (Fig. S2 and S3†).

All DSC traces of compounds 1-5 as E and Z forms are recorded to monitor their phase transitions and thermal isomerization as shown in Fig. S4.† Thermal parameters including the melting, crystallization, and cold-crystallization temperatures for E and Z isomers of all compounds are shown in Table 1, and the corresponding phase transition enthalpies are summarized in Table S1.† The distinct phases of E and Z isomer of compounds 1, 2, and 4 are exemplified by differential scanning calorimetry (DSC) in Fig. 2a. The E isomer of the compounds exhibits clear melting and crystallization peaks that correspond to large latent heat absorption and release processes. These thermal characteristics are similar to those of pristine azobenzene equivalent (Fig. 1d) that exhibits a sharp $T_{\rm m}$ (75 °C) and $T_{\rm c}$ (60 °C), reported by Grossman and coworkers.³⁷ The Z isomer of compound 2, on the other hand, shows a stable liquid phase between -40 °C and 110 °C, an extremely large window of temperatures defined by the partial crystallization point at the low end and by the onset of thermal reverse isomerization (Z-to-E) at the high end (Fig. 2a). The Z isomers of compounds 1 and 4 similarly display a stable liquid phase at room temperature. This is in contrast to the thermal behavior of pristine Z azobenzene equivalent which exhibits crystallinity at room temperature with distinct $T_{\rm m}$ (60 °C) and $T_{\rm c}$ (10 °C).37 The evaluation of phase transitions of compounds 1, 2, and 4, o-substituted with F and Cl groups, suggests that steric hindrance imposed by these o-substituents hinders the molecular packing among *Z* isomers more than that among *E* isomers.

Compound 1 shows the highest energy storage density (70 kJ mol; 0.15 MJ kg⁻¹) among all compounds, due to the considerable crystallization enthalpy of E isomer and E-Z isomerization enthalpy ($\Delta H_{\rm iso}$) (Table 2). However, the orthosubstitution in compounds 1-5 generally results in a reduced $\Delta H_{\rm iso}$ compared to that of pristine azobenzene (41 kJ mol⁻¹). For o-fluorinated compound 1, this is attributed to the lowered energy of its Z isomer, caused by the reduced electronic repulsion in its HOMO orbital.33 The substitution of F by Cl has minimal effect on the $\Delta H_{\rm iso}$ of compounds 2, 4, and 5, consistent with the previously reported calculation results on the o-F/ Cl substituted azobenzenes.36 In the case of compound 3, the HOMO centered on the azo group is close to the electron-rich methoxy groups for E isomer geometry, which results in raising its energy level. Its isomerization to the Z isomer relieves this interaction, which explains the low ΔH_{iso} measured in our work and calculated by a previous work.39 The E isomer crystallization enthalpy (ΔH_c) of compounds 1-4 is slightly reduced from the ΔH_c of pristine azobenzene equivalent (48 kJ mol⁻¹),³⁷ due to the reduced van der Waals interactions, caused by the ortho substitution on azobenzene. Compound 5 is a liquid at room temperature.

Although the overall heat storage densities of the new compounds are lower than those of the pristine azobenzene equivalent (94 kJ mol⁻¹)³⁷ or recently reported arylazopyrazole counterparts (76–120 kJ mol⁻¹),^{27,28} the new compounds are unique in that visible-range filtered sunlight of low irradiance

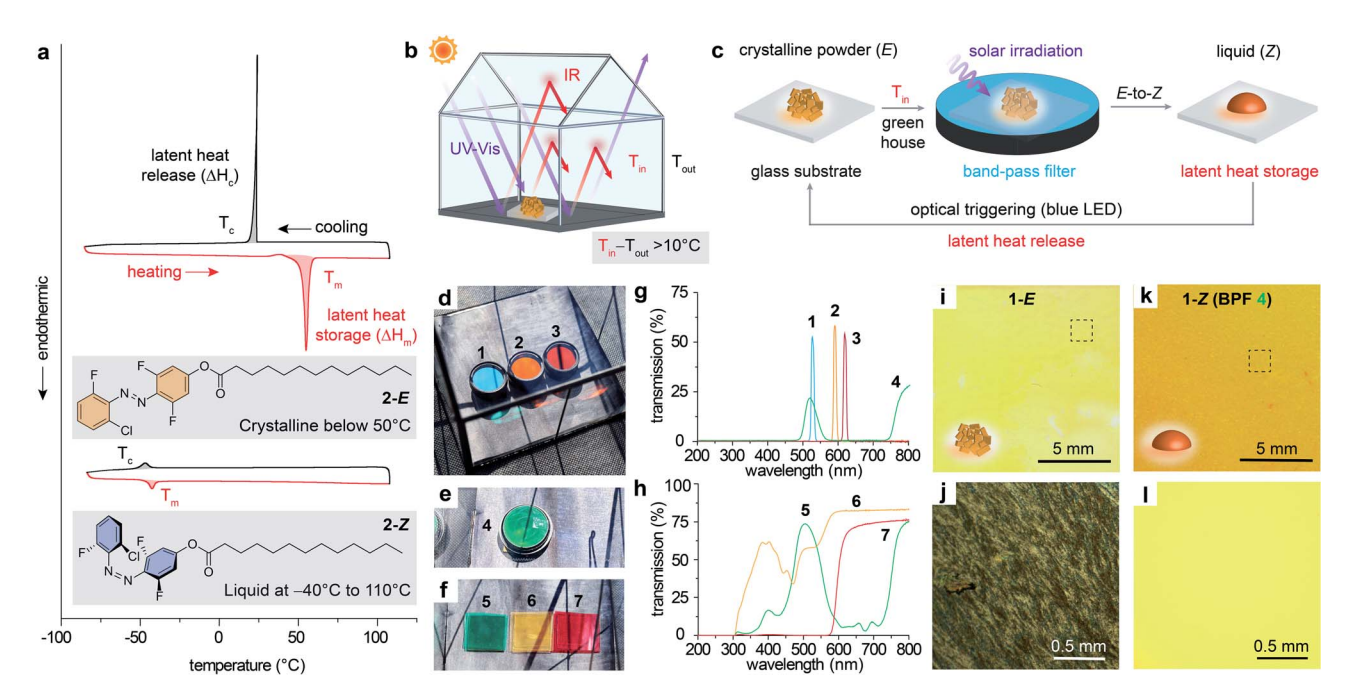


Fig. 2 (a) Differential scanning calorimetry plots of E and Z isomers of compound 2 as a representative example of compounds 1, 2 and 4. (b) A greenhouse setup under natural solar irradiation which allows for the UV-vis photon absorption by the compound at an elevated temperature. (c) A schematic illustration of the simultaneous phase transition and E-Z isomerization induced by the solar heat and visible-light-range solar irradiation through a band-pass filter. The initial crystalline E sample is regenerated after the optically-triggered heat release from the liquid Z by the blue LED (430 nm) irradiation. (d-f) Optical images of band-pass filters (BPF 1-7) used in the experiments. (g and h) UV-vis transmission spectra of BPF 1-7. (i) An optical image of a crystalline film of compound 1-E. (j) A magnified microscope image of the boxed area in (i). (k) An optical image of a liquid film of compound 1-Z after the solar irradiation through BPF 4 in the greenhouse for 5 hours. (I) A magnified microscope image of the boxed area in (k).

allows them to store photon and thermal energy. In contrast, all of the precedents require the photo-activation by a highintensity UV light source. Our strategy focuses on red-shifting the optical absorbance of photochromes to enable spontaneous energy storage under the filtered sunlight and concurrently achieving high thermal stability of Z isomers. This is demonstrated by their $T_{\rm iso}$ in the range of 105–120 °C as shown in Table 2, which is higher than that of pristine azobenzene equivalent (70 °C)37 and similar to those of arylazopyrazole counterparts (64-120 °C).27,28

In contrast to compounds 1, 2, and 4, the other two compounds 3 and 5 exhibit a same-phase E-Z isomerization due to the similar phase characteristics of E and Z isomers. Therefore, only $\Delta H_{\rm iso}$ is reliably stored in these two compounds through photo-isomerization, even though their E isomers undergo cold-crystallization which is difficult to rapidly trigger by photo-irradiation. The DSC traces of compound 3 as both Eand Z forms show the extensive supercooling of the molten phase to -80 °C (Fig. S4†), presumably due to the significantly reduced planarity of azobenzene from the o-methoxy substitution. Therefore, the photo-induced *E–Z* isomerization occurs in a supercooled liquid phase at room temperature, which can be achieved by the exposure to either filtered sunlight, LED, or fluorescent light. The Z liquid phase is more stable than E liquid at room temperature: the cold-crystallization temperature of Zisomer is 41 $^{\circ}$ C, while that of *E* isomer is 16 $^{\circ}$ C, therefore the *E*

isomer of compound 3 would cold-crystalize, releasing thermal energy over time. Compound 5 is intrinsically liquid at room temperature as synthesized, and both E and Z isomers remain liquid even at -80 °C. The E isomer shows minor coldcrystallization at −1 °C but immediately recovers the liquid phase at 9 °C. Thus, compounds 5 undergoes an unhindered E-Z photo-switching in the liquid phase at room temperature.

We demonstrate the spontaneous energy storage in the new compounds placed in a greenhouse (Fig. 2b) where the UV-vis range of sunlight transmitted through glass windows activates the E-to-Z switching, and the reflected thermal radiation in the

Table 2 Thermal parameters of Z-to-E isomerization and the E isomer crystallization for compounds $1-5^a$

	T _{iso} (°C)	$\Delta H_{\rm iso}$ (kJ mol ⁻¹)	$\Delta H_{\rm c}$ (kJ mol ⁻¹)	ΔH _{total} (kJ mol ⁻¹)/(MJ kg ⁻¹)
1	114	25	45	70/0.15
2	114	23	43	66/0.14
3	120	6	35 ^{cc}	41/0.08
4	109	25	37	62/0.12
5	105	21	7 ^{cc}	28/0.07

^a $T_{\rm iso}$: onset temperature of Z-to-E thermal reverse isomerization, $\Delta H_{\rm iso}$: isomerization enthalpy, ΔH_c : crystallization enthalpy of E isomer, cc: cold-crystallization, ΔH_{total} : total thermal energy released by the photo-triggered crystallization, calculated as the sum of $\Delta H_{\rm iso}$ and $\Delta H_{\rm c}$.

IR range facilitates the concomitant melting of the compounds (Fig. S5 \dagger). This is a stand-alone setup without any electrically-powdered light sources such as arc lamps or LEDs, which simultaneously harnesses solar photons and solar thermal energy. Fig. 2c illustrates the energy storage process in which the initial crystalline sample (E isomer) melts and isomerizes under the filtered sunlight. A commercial band-pass filter is used to allow for the transmission of light that selectively promotes E-to-Z switching, and the elevated temperature in the greenhouse assists the latent heat storage. The experiments were conducted in daylight when ambient temperature ranges from 25 °C to 33 °C (Table S2 \dagger).

In order to achieve an effective *E*-to-*Z* switching *via* the selective activation of $n-\pi^*$ band of *E* isomer, we tested a variety of band-pass filters (BPF, Fig. 2d–f) that were placed over the samples. The corresponding transmission spectra of the BPFs display various widths of transmitted wavelengths (Fig. 2g and h): BPFs 1–4 have narrower widths compared to BPFs 5–7 that are common colored transparency films. The comparative optical images of compound 1 film before and after the BPF 4-filtered solar irradiation in the greenhouse (Fig. 2i–l) demonstrate the clear morphological and color changes associated with the isomerization. A control experiment of photoswitching azobenzene and arylazopyrazole compounds (Fig. 1d) using a UV BPF was unsuccessful under a comparable greenhouse condition due to the lower UV irradiance in natural solar spectrum (Table S2†).

Fig. 3a depicts the increasing extent of *E*-to-*Z* isomerization of compound 1 by the varied irradiation time at 530 nm. The light intensity of 530 nm LED used for the experiment (5.55 mW) is 2-4 times higher those of the filtered sunlight through BPF 1 and 4 (estimated to be 1.46 mW and 2.49 mW, respectively; see Fig. S6-S8 \dagger). % Z in the film sample increases exponentially, reaching the saturation in 10 min of irradiation (Fig. S9 \dagger). Thus-formed liquid films containing various % Z isomers were monitored closely to measure the stability of liquid phase before crystallization, or the latent heat storage time. The short-irradiated films (1, 2, and 3 min) containing less than 70% Z isomer crystallized in 1, 3, and 8 days, respectively. Remarkably, other samples that were irradiated for 5 min or longer accumulated more than 70% Z isomer, and their liquid phase was preserved for at least a month in dark, demonstrating the exceptionally long-term storage of latent heat (Fig. S10†). Upon the extended observation of the stable liquid samples with more than 80% Z isomer, we measured the maximum heat storage time to be 59 days, nearly two months. We examined the half-lives $(t_{1/2})$ of the metastable Z isomers for compounds 1-4 in solution (Fig. S11 and Table S3†). The $t_{1/2}$ of 1-4 measured at 25 °C ranges from 258 days to 8.7 years, which reflects a significantly enhanced thermal stability of ortho-functionalized azobenzene Z isomers compared to pristine azobenzene ($t_{1/2}$ of 1.4 hours) and azobenzenes covalently bound to carbon support or polymer matrix ($t_{1/2}$ of 1–255 days).⁴⁰ The $t_{1/2}$ of 1–4 measured at 50 °C is also considerable, i.e. 9 to 40 days, enabling a long-term

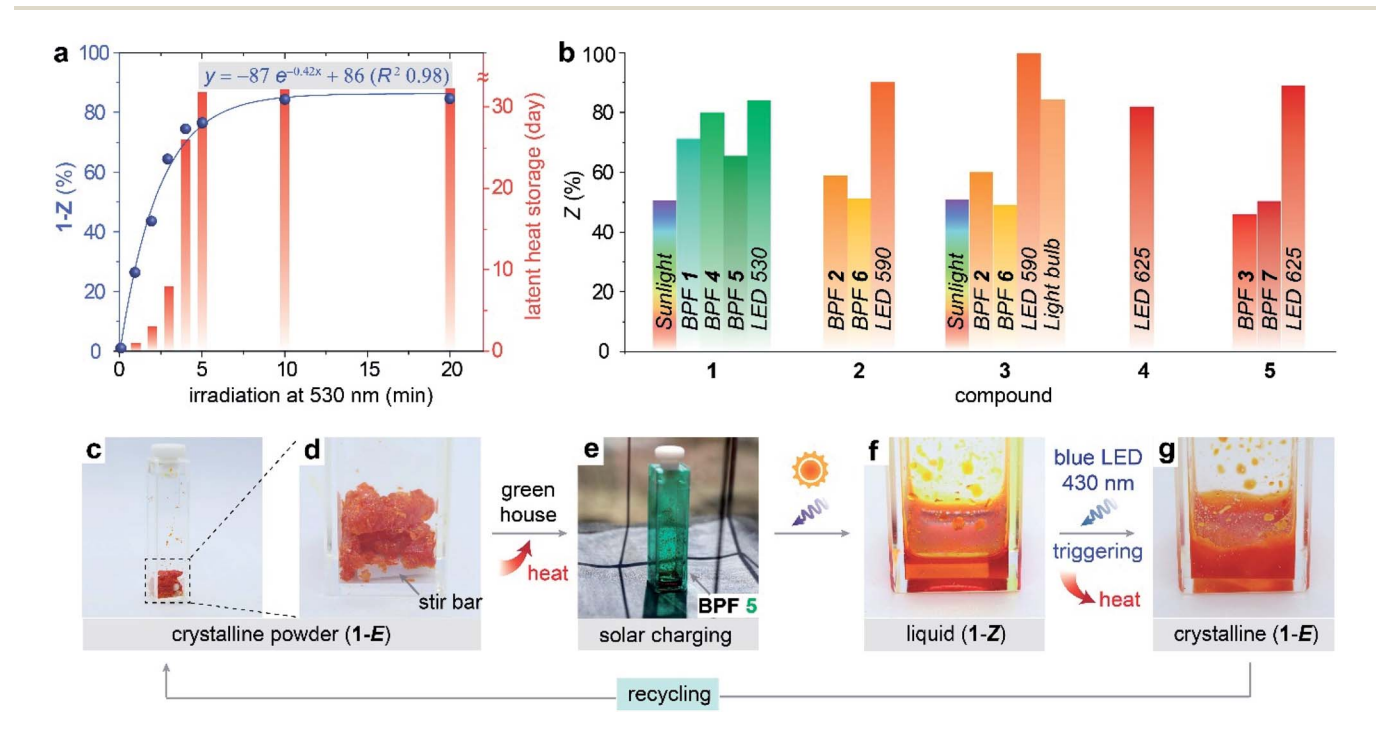


Fig. 3 (a) Increasing ratio of Z isomer (%) in films of compound $\mathbf{1}$ exposed to 530 nm LED at 50 °C. Each irradiated sample formed a liquid phase which was stable for various durations (i.e. latent heat storage time) before crystallizing. (b) The maximum % Z of compounds $\mathbf{1}-\mathbf{5}$ achieved by the unfiltered and band-pass-filtered solar irradiation or external light source (LED and fluorescent light bulb) illumination. Each result is color-coded according to the wavelength of peak transmission of each band-pass filter or the peak emission of each light source. (c-g) The process of solar energy storage by a crystalline powder sample ($\mathbf{1}-\mathbf{E}$) in a magnetically-stirred container covered by BPF 5 and placed in a greenhouse. The entire sample turned liquid containing 72% Z isomer within 5 hours of exposure to sunlight at 31 °C ambient temperature. The liquid phase solidified within the 15 min exposure to blue LED light while being stirred for the uniform exposure.

thermal energy storage and release in a closed system placed in an environment with fluctuating ambient temperatures. 41

Fig. 3b shows the % Z acquired for each compound by the direct sunlight, filtered sunlight, LED, and fluorescent light irradiation. We note that the experiments were conducted in a greenhouse, for direct or filtered sunlight irradiation, or under an ambient condition for the fluorescent light bulb illumination. The LED experiments were performed at temperatures a few degrees above the melting point of each E isomer to achieve the maximum % Z: 50 °C for compound 1, 60 °C for compound 2, and 80 °C for compound 4 (Table S4†). Due to the high melting point and crystallinity of compound 4, its conversion to Z isomer was negligible at room temperature or an elevated temperature in a greenhouse under direct or filtered sunlight. The photo-irradiation experiments on compounds 3 and 5 were performed at room temperature in a supercooled liquid (3) or liquid (5) phase. Interestingly, a fluorescent light bulb was more effective at isomerizing compound 3 than the direct or filtered sunlight. The complete experimental data on Eto-Z and Z-to-E conversion in solutions as well as condensed phases are summarized in Tables S4 and S5.† The LED emission profiles in Fig. S12† display wider widths than those of filtered sunlight (Fig. 2g).

It is notable that compound 1 achieves a high level of % Z in thin films under the filtered sunlight through BPF 4 (81%), similar to the maximum % Z acquired by 530 nm LED irradiation (84%), despite \sim 2.2 times lower intensity of the filtered sunlight. In contrast, compounds 2, 3, and 5 show a larger difference of % Z between the sunlight-irradiated and LED-

activated samples. This is primarily caused by the low absorption coefficient of E isomers at 590 nm and 625 nm (Fig. S1†), which requires a strong light source for achieving high % Z within a reasonable timeframe (e.g. hours). The radiant flux of filtered sunlight through BPF 2 or 3 is very low (1.56 and 1.52 mW; Fig. S6†) compared to those of LEDs. In addition, the actual flux is anticipated to be even lower than the calculated values based on AM 1.5 condition due to the intermittent radiation from natural climate. In the pursuit of achieving a higher % Z, we attempted irradiating compound 2 under sunlight through BPF 1 (530 nm), but 58% conversion was obtained as nearly identical to the results of BPF 2 and 6 (Table S5†).

The crystal-to-liquid phase transition at a larger scale (160 mg, 0.5-1 cm thick sample) than the thin film condition (\sim 5 µm) was demonstrated by a stirred sunlight irradiation of 1-E in the greenhouse through BPF 5 which provides a broad transmission of 450-600 nm (Fig. 3c-e). The conversion was successful, resulting in 72% Z within 5 hours of exposure to sunlight. The obtained liquid phase shows a similar viscosity to water rather than glycerol, as measured by strain sweep and frequency sweep rheometry (Fig. S13†). The low viscosity of the organic liquid opens up new opportunities in achieving a largequantity solar energy storage in such materials by employing a flow system, as previously demonstrated on solution-state norbornadiene42 (fulvalene)diruthenium43 and MOST compounds. The viscosity of molten 1-E was measured to be similar to that of liquid 1-Z, suggesting that sunlight-driven E-Zswitching could be achieved in the liquid flow system at

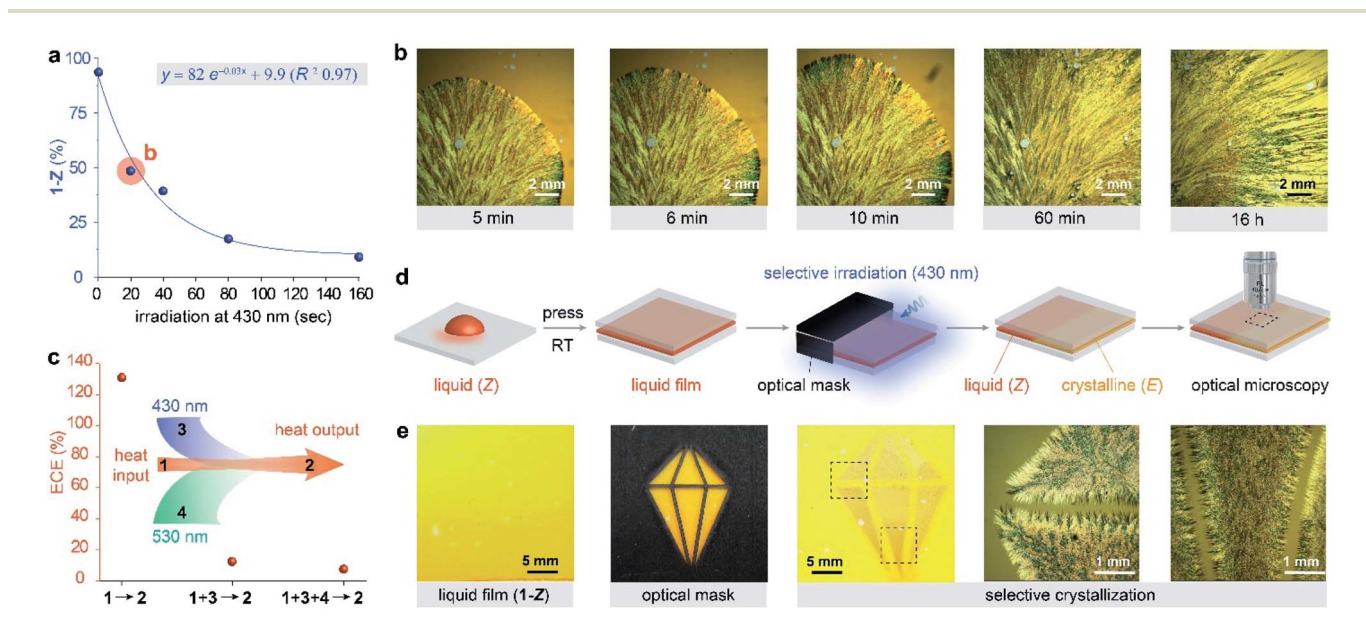


Fig. 4 (a) Decreasing ratio of Z isomers (%) in the liquid films of compound 1 exposed to 430 nm LED at room temperature. Upon 20, 40, 80, and 160 s irradiation, each liquid film crystallized after various delays. 80 s and 160 s irradiated films crystallized immediately. (b) A 20 s-irradiated film containing more than 50% E showed a relatively slower nucleation and gradual crystal propagation which was captured by optical microscopy of the identical sample area. (c) Energy conversion efficiency (ECE, %) calculated for the latent heat storage and release, showing the large heat output than input, as well as substantially larger photon energy input required for photo-switching. (d) A schematic illustration of the selective photo-induced crystallization process of liquid sample. (e) Optical microscope images of a liquid film before and after selective crystallization via 430 nm irradiation, showing a clear distinction between the irradiated and covered areas of sample. The dotted boxes mark the areas that are further magnified under the microscope and shown on the right.

elevated temperatures. The acquired liquid 1-Z was then triggered by 430 nm blue LED to immediately crystallize and release heat (Fig. 3f and g). The crystallized material containing 91% E isomer after the heat release was recycled for energy storage in the greenhouse.

This heat release process was successfully monitored and recorded by an IR thermal camera (Videos S1, S2 and Fig. S14†). We observe the immediate heat release from the liquid 1-Z during the crystallization upon the exposure to 430 nm, as the temperature of the sample rises up to 23 °C which is consistently 2-3 °C higher than the surroundings. We note that the irradiance of the 430 nm LED (3.5 mW cm⁻²) used in our crystallization experiments is significantly lower than that of the laser (110 mW cm⁻²) employed in a recent work reporting similar processes.²⁷ Considering the low-intensity optical trigger and the rapid heat dissipation to the cooler surroundings from the heat-releasing materials (160 mg), the 2-3 °C rise in temperature detected by the IR camera is significant. This infers that a more considerable temperature change will be achievable in a larger-scale experiment equipped with thermal insulation around the PCM. After the complete crystallization, the temperature drops to 19-20 °C, quickly reaching a thermal equilibrium. The control experiment in which the solid 1-E is irradiated by 430 nm LED showed no change of temperature (Video S3†), indicating that the LED-induced IR emission from the ground-state photochrome is negligible. This confirms that the appreciable temperature change observed from 1-Z is primarily the result of the crystallization and concurrent release of excess chemical potential (i.e. Z-to-E isomerization enthalpy). The mechanical stirring does not contribute to any measurable temperature change, as we detect a constantly low temperature of stirred liquid 1-Z before 430 nm irradiation (Video S2 and Fig. S14†).

As demonstrated in the IR thermal imaging, the crystallization of liquid Z samples and the consequent heat release are effectively triggered by the irradiation of 430 nm LED. The n- π^* band of all Z isomers (compounds 1-5) peaks at 424 \pm 6 nm, thus the Z-to-E reverse isomerization occurs fast under 430 nm irradiation. Fig. 4a shows a rapid exponential decrease of % Z in the liquid films of compound 1 upon 430 nm exposure. Even within 20 s of irradiation, over 50% conversion to E isomer is obtained, and after 80 s the % Z drops below 20% (Fig. S15†) inducing an immediate and complete crystallization. Since the crystallization is very rapid, it was challenging to monitor the nucleation and propagation processes. Thus, we selected a sample (2.5 cm by 2.5 cm film) that is irradiated only for 20 s to observe the growth of crystals under an optical microscope (Fig. 4b). The partial crystallization is observed after 5 min past the initial irradiation, which reflects the slow assembly of Eisomers in the liquid sample still containing \sim 50% Z isomers. The initial nucleation site propagates slowly over 60 min due to the low concentration of E isomers. After 16 hours, the crystalline phase becomes denser and thicker, while there is still liquid phase surrounding the crystals. This corroborates the long-term stability of Z liquid in dark (Fig. 3a) and the high thermal reversion temperature for Z-to-E isomerization (onset $T_{\rm iso}$ ~114 °C, Fig. S4† and Table S1†).

In addition, the crystallization of liquid **1-Z** was successfully demonstrated by the exposure to filtered sunlight through a 430 nm BPF, despite the slower kinetics of reversion and crystallization compared to those of LED-triggered isomerization. We observed the initial crystallization in 15 min and its completion in 1 hour. This indicates a potential to achieve a complete heat storage and release cycle using the new compounds without any usage of artificial light sources (Fig. S16†).

Based on the measurement of the heat absorption, heat release, and photon absorption needed for isomerization, we calculated the energy conversion efficiency (ECE, %) of the optically-controlled energy storage materials. The relative energy input and output are shown in Fig. 4c for compound 1 as an example. The melting enthalpy of 1-*E* is obtained by integrating the DSC endothermic peak of melting transition (*i.e.* heat input). The heat output was calculated as the sum of the crystallization enthalpy of 1-*E* and the isomerization enthalpy released from *Z*-to-*E* reversion. The thermal energy storage efficiency, the ratio of heat output and input, thus exceeds 100% due to the additional isomerization enthalpy released during the optically-triggered crystallization (*i.e.* 131%).

The photon energy required to trigger the crystallization was calculated by applying the quantum yield of Z-to-E switching. Due to the suboptimal quantum yield of o-fluoroazobenzene $(\Phi_{Z-E} = 0.49)^{33}$, significant photon absorption is required for inducing crystallization. Therefore, the ECE, the ratio of heat output and the total photon and heat input, decreases to \sim 13%. Furthermore, considering the incident photon energy for E-to-Z conversion, the total ECE drops to \sim 6% due to the low quantum yield of isomerization ($\Phi_{E-Z}=0.3$).³³ These ECEs describe the molecule's intrinsic capability of storing thermal energy under optical control by monochromic light sources. By taking into consideration of the fractional solar irradiance used for the Eto-Z switching upon the filtration through BPF 4 (i.e. 1.3%), we obtained the efficiency of 0.14% for compound 1. The ECE calculations of all compounds are summarized in ESI, Note 1 and Table S6.†

Additionally, we calculated a solar energy storage efficiency of compound 1 under AM 1.5 solar irradiation, according to a reported procedure used for other azobenzene MOST compounds (ESI, Note 2†). 24,27,44 Considering the entire solar spectrum as the energy input, the efficiency of 0.75% is obtained, within the range of the previously-reported values for azobenzene MOST (0.25–1.28%) and higher than the ECE (0.14%) calculated by our method that considers stepwise heat input, phase transition, and photo-activation involved in controlling the heat storage in PCMs. The solar energy storage efficiency of compound 1 for the filtered sunlight (BPF 4) as the energy input is calculated to be 5.54%.

The photo-induced crystallization process is further manifested by the selective exposure of the *Z* isomer in liquid phase to 430 nm LED through an optical mask (Fig. 4d). The interface between the exposed and covered area is investigated by optical microscopy to confirm that the crystallization is solely induced by photo-irradiation rather than nucleation from any artifact. Fig. 4e clearly visualizes the selective irradiation process and the

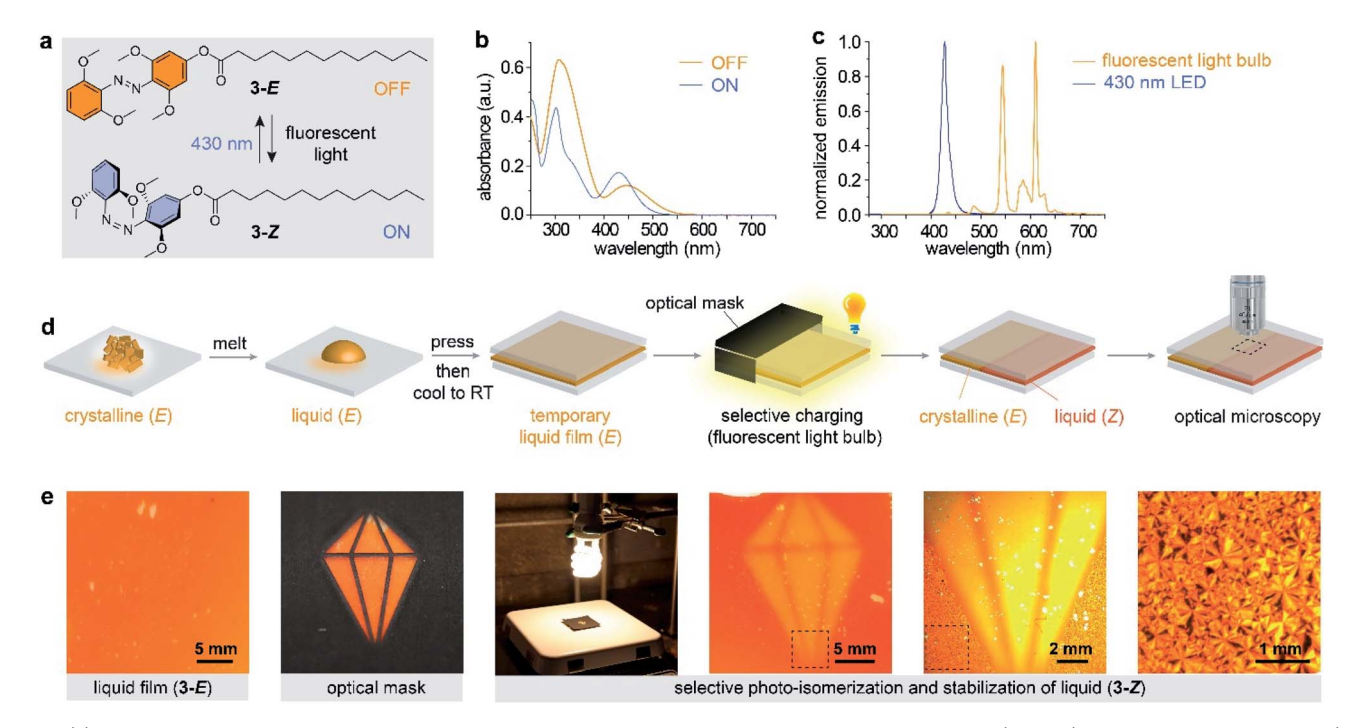


Fig. 5 (a) Reversible structural isomerization of compound 3 by an unfiltered fluorescent light irradiation (E-to-Z) and blue LED illumination (Zto-E). (b) UV-vis absorption spectra of as-synthesized compound 3 (OFF) as well as the compound switched to Z isomeric form (ON). (c) The normalized emission of a fluorescent light bulb and a blue LED used in the experiments. (d) A schematic illustration of the selective photoswitching of the supercooled liquid 3-E. (e) Optical microscope images of the liquid film before and after selective fluorescent light irradiation for 90 min, showing a clear distinction between the irradiated 3-Z (liquid) and covered 3-E (crystallized) areas of sample. The dotted boxes mark the areas that are further magnified under microscope and shown on the right.

interface between the generated crystalline phase and intact liquid phase. The intricate crystal pattern is preserved for at least a month without any visible propagation of the crystals, confirming that only *E* isomers are able to crystallize, consistent with the long-term stability of Z liquid phase (Fig. 3a). Therefore, the crystal propagation observed in Fig. 4b implies the delayed assembly of E isomers that are intermixed with Zisomers (\sim 50%) in the film after the brief, uniform exposure to blue light.

Surprisingly, all compounds 1–5 were able to undergo E-to-Z isomerization by the exposure to a regular fluorescent light bulb (Table S4†), which suggests a potential to develop energy storage materials that not only harness sunlight but also indoor ambient light. Compound 3 was selected to demonstrate the fluorescent light-induced E-to-Z switching (Fig. 5a), since compound 3 showed a considerably larger % Z acquired by fluorescent light than filtered sunlight irradiation (Fig. 3b). Due to the red-shifted $n-\pi^*$ band of 3-E (Fig. 5b), the fluorescent light bulb emission centered around 550 nm and 610 nm (Fig. 5c) effectively promoted *E*-to-*Z* conversion. The reversion is achieved by 430 nm irradiation, which has a negligible overlap with the bulb emission profile.

The experimental procedure is illustrated in Fig. 5d. Compound 3-E forms a supercooled liquid at room temperature upon pre-melting, and the liquid film is exposed to fluorescent light through an optical mask. 3-Z isomer is generated by the selective irradiation and form a stable liquid phase (the thermal half-life of 3-Z exceeds 8 years at room temperature, see

Fig. S11† and Table S3†), while the supercooled 3-E gradually cold-crystallizes during the 90 min experiment. The optical microscope images in Fig. 5e show a clear contrast between the liquid Z isomers and crystalline E isomers. This shows the possibility of utilizing compound 3 among others as a PCM that harnesses photons from indoor fluorescent light and release latent heat upon triggering by a blue LED.

We note that a light penetration depth of condensed phase materials is shorter than that of dilute solution, due to the spectral overlap between E and Z isomers, which limits the thickness of films that can be fully photoswitched. The maximum penetration depths for representative compounds 1 and 3 were determined as 349 and 108 µm, respectively, for 530 and 590 nm wavelength (Fig. S17-S20 and ESI, Note 3†). Optical profilometry was used to confirm the uniform thickness of films prepared by the melt-press method (Fig S21-S26†). Nevertheless, as shown in Fig. 3e, condensed phase samples of 0.5-1 cm thickness could photoswitch to achieve 72% Z isomer by being stirred continuously under irradiation. This highlights a way in which a large quantity of condensed phase materials could be optically activated for practical applications despite the short light penetration depth.

3. Conclusions

The newly designed compounds demonstrated to undergo sunlight-driven E-to-Z isomerization and simultaneous solid-toliquid transition, storing both isomerization energy and latent heat in the liquid phase, without the need for high-intensity UV sources or external heat sources. The liquid phase containing maximum % Z is preserved for nearly two months in the absence of crystallization, exhibiting a remarkable stability and the long-term storage of thermal energy. The rapid release of the stored energy prompted by a blue LED irradiation was clearly monitored by an IR thermal camera. The compounds also revealed the potential to recycle the photon energy from indoor fluorescent light illumination. These successful demonstrations signify the utility of photo-responsive organic materials for solar energy harvesting, as a complementary tool to photo-voltaics and photocatalysis.

4. Experimental

4.1 Synthesis and characterization

Compounds 1–5 were prepared by the azo coupling between substituted phenols and anilines, followed by the Steglich esterification. ^{45,46} The detailed synthetic procedures and the characterization data including HRMS and ¹H, ¹³C, and ¹⁹F NMR spectra of intermediates and products are included in ESI.†

For purification, flash silica gel column chromatography was performed using CombiFlash RF automated flash chromatography system with Merck Silica Gel 60 (230–400 mesh). ¹H, ¹³C, ¹⁹F NMR spectra were recorded on a Bruker Avance 400 Spectrometer at 400 MHz, 100 MHz, and 376 MHz, respectively. Tetramethylsilane (TMS) was used as an internal standard for ¹H and ¹³C spectra, and trifluoroacetic acid was used as an external standard for ¹⁹F spectra. ESI-HRMS were recorded at University of Illinois at Urbana-Champaign Mass Spectrometry Lab with a Waters Synapt G2-Si ESI mass spectrometer. Optical microscope images were taken with Olympus Q-Color 3 imaging system installed on the Olympus SZ-40 Stereo Microscope with Olympus SZ-PO Polarizing Lens and Schott ACE Light Source with EKE Lamp.

4.2 UV-vis absorption spectroscopy

All UV-vis absorption spectra were obtained using a Varian Cary 50 UV-vis Spectrophotometer in a UV Quartz cuvette with a path length of 10 mm. All the *E* isomers were dissolved in chloroform at 0.0125 mg ml $^{-1}$ concentration. The UV-vis spectra of the *E* isomers were first recorded, then the compounds were irradiated with light sources until they reached a photostationary state (PSS). LED light sources include Thorlab M395L4 (395 nm, 6.7 μ W mm $^{-2}$), M430L4 (430 nm, 35.3 μ W mm $^{-2}$), M530L3 (530 nm, 9.5 μ W mm $^{-2}$), M590L4 (590 nm, 6.0 μ W mm $^{-2}$), and M625L4 (625 nm, 21.9 μ W mm $^{-2}$). The fluorescent light source was a GE 13W FLE13HT3/2/SW light bulb.

For isomerization cycling experiments, compounds **1–5** dissolved in chloroform were exposed to alternating irradiation of 530 nm for 50 s and 430 nm for 20 s at 20 °C. The absorption at the $\lambda_{\rm max}$ of E isomer was recorded to monitor the cyclic performance of compounds. A 530 nm LED was chosen as the common light source inducing E-to-Z isomerization because of its favorable photo-isomerization kinetics, although other light

sources could achieve a higher PSS for compounds 2–5. For photo-stability tests, compounds 1–5 dissolved in chloroform were continuously irradiated by 530 nm LED for 1000 min at 20 °C. The absorption at the λ_{max} of *E* isomer was recorded every 10 min.

4.3 DSC measurements

Solution-state *Z* isomers were prepared from corresponding *E* isomers in dichloromethane which were irradiated with a suitable light source until PSS was reached. The solutions were then concentrated and dried under high vacuum.

The prepared Z isomers as well as the E isomers were transferred to DSC for thermal property measurements. DSC experiments were recorded on a DSC 250 (TA Instruments) with an RSC 90 Refrigerated Cooling System. The cooling and heating rates during DSC experiments were set to 10 °C min⁻¹ unless specified in figure caption. In order to measure thermal reverse isomerization, all Z isomers were heated to 190 °C.

4.4 Thin film experiments

Since crystalline azobenzene materials hardly form a uniform film by solution casting, we prepared the films by a melt-press method. Z-rich and E-rich thin films were prepared by placing 5 mg of E-rich or Z-rich sample on a 2.5 cm by 2.5 cm glass slide. Solid samples were heated above $T_{\rm m}$, covered by another glass slide, then cooled to RT. Liquid samples were directly covered by another glass slide at RT. The molten solid or liquid was spread by the cover glass to fill the entire area between the glass slides.

To show the selective crystallization, an optical mask was placed on 1-Z film which was then irradiated with a 430 nm LED for 90 s at RT. After the irradiation, the mask was removed, and the film was observed under an optical microscope. To show the selective isomerization of 3-E, a thin film of molten 3-E was prepared. The film was supercooled to RT, covered with a mask, and irradiated with a fluorescent light bulb for 90 min. After the irradiation, the mask was removed, and the film was observed under an optical microscope.

Four identical Z-rich thin films of 1 were prepared for the measurement of Z-to-E time-dependent isomerization. Each film was irradiated with 430 nm light at RT for 20, 40, 80, and 160 s, respectively. The percentage of Z isomer was measured using 1 H NMR.

Likewise, seven identical E-rich thin films of $\mathbf{1}$ were prepared for the measurement of E-to-Z isomerization. Each film was irradiated with 530 nm light at 50 °C for 1, 2, 3, 4, 5, 10, and 20 min, respectively. The percentage of Z isomer was measured using 1 H NMR. To determine the heat storage time, the identical procedure was carried out to prepare liquid Z samples that were monitored in dark until crystallization occurs.

4.5 Solar irradiation experiments

For greenhouse experiments, smaller films were made with 2 mg sample on 1.6 cm by 1.6 cm substrates to accommodate the band-pass filter coverage. A VWR advanced hot plate stirrer

was used for the stirred-irradiation process and auxiliary heating as necessary.

The greenhouse is composed of a metal frame and glass walls, and a black piece of paper was placed on the bottom of the greenhouse. An E-rich film was placed on the paper with a different filter covering the entire substrate. Three types of filters were used: Thorlab bandpass filter of 360 nm (UV), 530 nm (BPF 1), 590 nm (BPF 2), 620 nm (BPF 3) (Thorlab model: FB360-10, FB530-10, FB590-10, FB620-10); Roundshaped color filter from Ultrafire A100 (green) (BPF 4); Flexible color filter from Neewer (green, orange, red) (BPF 5, 6, 7). Zrich films of compound 1 were used for the reverse isomerization experiment by the filtered sunlight through a 430 nm (FB430-10) BPF.

The films were exposed to sunlight under each filter for 5 hours unless specifically addressed. After irradiation the material was dissolved in CDCl₃, and % Z was measured by ¹H NMR. The bulk sample isomerization was conducted with 160 mg of crystalline compound 1 and a stir bar added to a UV Quartz cuvette with a pathlength of 10 mm. The cuvette was placed on the black paper, and a stir plate was placed under the greenhouse. The cuvette was wrapped with one layer of the flexible green filter (BPF 5). After 10 min, 1 was fully melted and continuously irradiated with sunlight in the greenhouse for 5 hours being stirred at 300 rpm. ~5 mg aliquot of 1 was taken out for ¹H NMR analysis.

4.6 Optical characterization of light sources and substrates

The emission spectrum of the fluorescent light bulb was measured with a Shimadzu RF-5301 Fluorimeter, following the procedure from Shimadzu.47 The irradiation power of various light sources was measured using a Thorlab PM160T Thermal Sensor Power Meter at the wavelength of maximum output intensity. The transmission spectra of substrates were measured with a Varian Cary 50 UV-vis Spectrophotometer.

Rheology measurements

The strain sweep measurement was conducted using a TA Instruments ARES-G2 rheometer with Parallel Plate System. The strain sweep was measured at angular frequency of 6.28 rad s⁻¹ at RT for 290 s, except for 1-E which was measured at 45 °C. The gap between plates was 0.4 mm for all measurements.

4.8 IR thermal imaging

All IR videos and images were recorded at 1 frame per sec with Avio InfRec R450P IR camera equipped with a standard lens, capable of measuring a temperature range from -40 to 120 °C. At RT, a stir bar and 160 mg of 1 were placed in a UV Quartz cuvette with a pathlength of 10 mm. 1-Z was monitored in Video S1 & S2† to demonstrate the heat release, and 1-E was monitored as a control. The cap of the cuvette was removed, and the IR camera was set on top of the cuvette to record the top-down view of samples in the cuvette through the top opening. 430 nm LED was placed \sim 20 cm away from the side of the cuvette, irradiating directly on the substrate. The total duration of Video S1† was 25 min during which the LED was kept on. The total duration of Video S2† was 30 min, and the LED was switched on at 0' 30" and off at 29' 30". The total duration of Video S3† was 5 min during which the LED was kept on. 300 rpm stirring was applied in Videos S1 and S2† by a VWR advanced hot plate stirrer.

4.9 Optical penetration depth measurement

We measured the light penetration depths of compounds 1 and 3 by preparing films of varied thickness (5-550 μm) and exposing them to 530 and 590 nm LED, respectively, over 3 h. The E-to-Z isomerization rate was measured by ¹H NMR characterization of the films after reaching PSS.

Films thinner than 100 µm were prepared using 5-45 mg of compound 1 or 3 by pressing the molten sample with a cover glass slide. Films thicker than 100 µm were prepared by melting 50-200 mg of sample in a thin glass well created by cover slip spacers then covering the well by another glass slide. The cover glass slide was lifted after the cooling of a liquid film to room temperature.

The thickness of each film was measured with Zeta-20 Optical Profilometer at 12 positions across the edges of the film. The films displayed overall uniform thickness across areas as large as $2.5 \text{ cm} \times 2.5 \text{ cm}$. Different objectives were used for the film with varied thickness: a 50× lens with a field of view (FOV) of 466 \times 349 μ m for films thinner than 10 μ m, a 20 \times or 10× lens with a FOV of 1165 \times 874 μm or 2327 \times 1745 μm for 10–100 μ m-thick films, and a 5× lens with a FOV of 4697 × 3522 μm for films thicker than 100 μm.

Conflicts of interest

There are no conflicts to declare.

Acknowledgements

The research was supported by the SPROUT award (2019-042) from Brandeis Office of Technology Licensing and Provost Research Award from Brandeis University. We also acknowledge support from Brandeis NSF MRSEC, Bioinspired Soft Materials, DMR-2011486. We thank Prof Bing Xu and Jiaqi Guo at Brandeis University for the helpful guidance on the rheometry experiments.

References

- 1 T. P. Yoon, Acc. Chem. Res., 2016, 49, 2307-2315.
- 2 R. Brimioulle, D. Lenhart, M. M. Maturi and T. Bach, Angew. Chem., Int. Ed., 2015, 54, 3872-3890.
- 3 N. Hoffmann, Chem. Rev., 2008, 108, 1052-1103.
- 4 F. Tong, W. Xu, T. Guo, B. F. Lui, R. C. Hayward, P. Palffy-Muhoray, R. O. Al-Kaysi and C. J. Bardeen, J. Mater. Chem. C, 2020, 8, 5036-5044.
- 5 M. Chen, B. Yao, M. Kappl, S. Liu, J. Yuan, R. Berger, F. Zhang, H. J. Butt, Y. Liu and S. Wu, Adv. Funct. Mater., 2020, 3, 1906752.

- 6 D. T. Nguyen, M. Freitag, C. Gutheil, K. Sotthewes, B. J. Tyler, M. Böckmann, M. Das, F. Schlüter, N. L. Doltsinis, H. F. Arlinghaus, B. J. Ravoo and F. Glorius, *Angew. Chem., Int. Ed.*, 2020, 59, 13651–13656.
- 7 H. Nie, N. S. Schauser, N. D. Dolinski, J. Hu, C. J. Hawker, R. A. Segalman and J. Read de Alaniz, *Angew. Chem., Int. Ed.*, 2020, 59, 5123–5128.
- 8 A. I. Hanopolskyi, S. De, M. J. Białek, Y. Diskin-Posner, L. Avram, M. Feller and R. Klajn, *Beilstein J. Org. Chem.*, 2019, 15, 2398–2407.
- A. H. Heindl and H. A. Wegner, *Beilstein J. Org. Chem.*, 2020,
 16, 22–31.
- 10 A. M. Rice, C. R. Martin, V. A. Galitskiy, A. A. Berseneva, G. A. Leith and N. B. Shustova, *Chem. Rev.*, 2020, **120**, 8790–8813.
- 11 A. H. Heindl and H. A. Wegner, *Chem.-Eur. J.*, 2020, **26**, 13730-13737.
- 12 L. Hou, T. Leydecker, X. Zhang, W. Rekab, M. Herder, C. Cendra, S. Hecht, I. McCulloch, A. Salleo, E. Orgiu and P. Samorì, J. Am. Chem. Soc., 2020, 142, 11050–11059.
- 13 K. Klaue, W. Han, P. Liesfeld, F. Berger, Y. Garmshausen and S. Hecht, J. Am. Chem. Soc., 2020, 142, 11857–11864.
- 14 P. Lentes, E. Stadler, F. Röhricht, A. Brahms, J. Gröbner, F. D. Sönnichsen, G. Gescheidt and R. Herges, J. Am. Chem. Soc., 2019, 141, 13592–13600.
- 15 S. Seshadri, L. F. Gockowski, J. Lee, M. Sroda, M. E. Helgeson, J. Read de Alaniz and M. T. Valentine, *Nat. Commun.*, 2020, 11, 2599.
- 16 J. Orrego-Hernández, A. Dreos and K. Moth-Poulsen, *Acc. Chem. Res.*, 2020, 53, 1478–1487.
- 17 Z. Wang, J. Udmark, K. Börjesson, R. Rodrigues, A. Roffey, M. Abrahamsson, M. B. Nielsen and K. Moth-Poulsen, *ChemSusChem*, 2017, 10, 3049–3055.
- 18 Z. Wang, R. Losantos, D. Sampedro, M. A. Morikawa, K. Börjesson, N. Kimizuka and K. Moth-Poulsen, *J. Mater. Chem. A*, 2019, 7, 15042–15047.
- 19 R. J. Corruccini and E. C. Gilbert, J. Am. Chem. Soc., 1939, 61, 2925–2927.
- 20 M. A. Gerkman and G. G. D. Han, Joule, 2020, 4, 1621-1625.
- 21 K. Ishiba, M. A. Morikawa, C. Chikara, T. Yamada, K. Iwase, M. Kawakita and N. Kimizuka, *Angew. Chem., Int. Ed.*, 2015, **54**, 1532–1536.
- 22 G. D. Han, S. S. Park, Y. Liu, D. Zhitomirsky, E. Cho, M. DincĂ and J. C. Grossman, *J. Mater. Chem. A*, 2016, 4, 16157–16165.
- 23 H. Zhou, C. Xue, P. Weis, Y. Suzuki, S. Huang, K. Koynov, G. K. Auernhammer, R. Berger, H. J. Butt and S. Wu, *Nat. Chem.*, 2017, **9**, 145–151.
- 24 A. K. Saydjari, P. Weis and S. Wu, *Adv. Energy Mater.*, 2017, 7, 1601622.
- 25 A. S. Kuenstler, K. D. Clark, J. Read De Alaniz and R. C. Hayward, *ACS Macro Lett.*, 2020, **9**, 902–909.
- 26 W. C. Xu, S. Sun and S. Wu, *Angew. Chem., Int. Ed.*, 2019, **58**, 9712–9740.

- 27 Z. Y. Zhang, Y. He, Z. Wang, J. Xu, M. Xie, P. Tao, D. Ji, K. Moth-Poulsen and T. Li, J. Am. Chem. Soc., 2020, 142, 12256–12264.
- 28 M. A. Gerkman, R. S. L. Gibson, J. Calbo, Y. Shi, M. J. Fuchter and G. G. D. Han, *J. Am. Chem. Soc.*, 2020, **142**, 8688–8695.
- 29 G. G. D. Han, J. H. Deru, E. N. Cho and J. C. Grossman, *Chem. Commun.*, 2018, **54**, 10722–10725.
- 30 H. Liu, L. Dong, H. Wang, T. Xu, W. Gao, F. Zhai, Y. Feng and W. Feng, *Adv. Funct. Mater.*, 2020, 2008496.
- 31 H. Liu, Y. Feng and W. Feng, *Composites Commun.*, 2020, 21, 100402.
- 32 Y. Jiang, J. Liu, W. Luo, X. Quan, H. Li, J. Huang and W. Feng, *Surf. Interfaces*, 2021, **24**, 101071.
- 33 C. Knie, M. Utecht, F. Zhao, H. Kulla, S. Kovalenko, A. M. Brouwer, P. Saalfrank, S. Hecht and D. Bléger, Chem.-Eur. J., 2014, 20, 16492–16501.
- 34 A. A. Beharry, O. Sadovski and G. A. Woolley, *J. Am. Chem. Soc.*, 2011, 133, 19684–19687.
- 35 S. Samanta, A. A. Beharry, O. Sadovski, T. M. McCormick, A. Babalhavaeji, V. Tropepe and G. A. Woolley, J. Am. Chem. Soc., 2013, 135, 9777–9784.
- 36 D. B. Konrad, G. Savasci, L. Allmendinger, D. Trauner, C. Ochsenfeld and A. M. Ali, J. Am. Chem. Soc., 2020, 142, 6538–6547.
- 37 G. G. D. Han, H. Li and J. C. Grossman, *Nat. Commun.*, 2017, 8, 1446.
- 38 D. Bléger, J. Schwarz, A. M. Brouwer and S. Hecht, *J. Am. Chem. Soc.*, 2012, **134**, 20597–20600.
- 39 A. A. Beharry, O. Sadovski and G. A. Woolley, *J. Am. Chem. Soc.*, 2011, **133**, 19684–19687.
- 40 C.-L. Sun, C. Wang and R. Boulatov, *ChemPhotoChem*, 2019, 3, 268–283.
- 41 T. J. Kurcharski, Y. Tian, S. Akbulatov and R. Boulatov, *Energy Environ. Sci.*, 2011, 4, 4449–4472.
- 42 Z. Wang, A. Roffey, R. Losantos, A. Lennartson, M. Jevric, A. U. Petersen, M. Quant, A. Dreos, X. Wen, D. Sampedro, K. Börjesson and K. Moth-Poulsen, *Energy Environ. Sci.*, 2019, 12, 187–193.
- 43 K. Moth-Poulsen, D. Ćoso, K. Börjesson, N. Vinokurov, S. K. Meier, A. Majumdar, K. P. C. Vollhardt and R. A. Segalman, *Energy Environ. Sci.*, 2012, 5, 8534–8537.
- 44 T. J. Kucharski, N. Ferralis, A. M. Kolpak, J. O. Zheng, D. G. Nocera and J. C. Grossman, *Nat. Chem.*, 2014, **6**, 441–447.
- 45 L. Li, S. Cui, A. Hu, W. Zhang, Y. Li, N. Zhou, Z. Zhang and X. Zhu, *Chem. Commun.*, 2020, 56, 6237–6240.
- 46 P. Weis, D. Wang and S. Wu, *Macromolecules*, 2016, **49**, 6368–6373.
- 47 Measurement of Emission Spectra of LED Light Bulbs, https://www.shimadzu.com/an/sites/shimadzu.com.an/files/pim/pim_document_file/applications/application_note/12062/jpa415028.pdf, accessed 12/11/2020.